Received: 1 August 2017 | Revised: 17 January 2018 | Accepted: 14 February 2018

DOI: 10.1111/bre.12282

ORIGINAL ARTICLE

WILEY Basin Research IAS EAGE

Submarine sediment routing over a blocky mass-transport deposit in the Espírito Santo Basin, SE Brazil

Nicholas I. P. Ward | **Tiago M. Alves** | **Thomas G. Blenkinsop**

3D Seismic Lab, School of Earth and Ocean Sciences, Cardiff University, Cardiff, UK

Correspondence
Nicholas I. P. Ward, 3D Seismic Lab, School of Earth and Ocean Sciences, Cardiff University, Cardiff, UK.
Email: wardni@cardiff.ac.uk

Funding information
Natural Environment Research Council

Abstract

The control of slide blocks on slope depositional systems is investigated in a high-quality 3D seismic volume from the Espírito Santo Basin, SE Brazil. Seismic interpretation and statistical methods were used to understand the effect of differential compaction on strata proximal to the headwall of a blocky mass-transport deposit (MTD), where blocks are large and undisturbed (remnant), and in the distal part of this same deposit. The distal part contains smaller rafted blocks that moved and deformed with the MTD. Upon their emplacement, the positive topographic relief of blocks created a rugged seafloor, confining sediment pathways and creating accommodation space for slope sediment. In parallel, competent blocks resisted compaction more than the surrounding debrite matrix during early burial. This resulted in differential compaction between competent blocks and soft flanking strata, in a process that was able to maintain a rugged seafloor for >5 Ma after burial. Around the largest blocks, a cluster of striations associated with a submarine channel bypassed these obstructions on the slope and, as a result, reflects important deflection by blocks and compaction-related folds that were obstructing turbidite flows. Log-log graphs were made to compare the width and height of different stratigraphic elements; blocks, depocentres and channels. There is a strong correlation between the sizes of each element, but with each subsequent stage (block–depocentre–channel) displaying marked reductions in height. Blocky MTDs found on passive margins across the globe are likely to experience similar effects during early burial to those documented in this work.

1 | INTRODUCTION

Mass-wasting is capable of transporting large volumes of sediment downslope and is one of the primary processes filling deep-water sedimentary basins around the world (Beaubouef & Abreu, 2010; Gamboa, Alves, Cartwright, & Terrinha, 2010; Gee, Gawthorpe, & Friedmann, 2006; Masson, Harbitz, Wynn, Pedersen, & Løvholt, 2006; Newton, Shipp, Mosher, & Wach, 2004; Omosanya & Alves, 2013). Mass-wasting on continental slopes usually occurs in the form of recurrent (*mass-transport complex*) or discrete (*mass-transport deposit*) events, as documented in Pickering and Hiscott (2015). Both types of events can remobilize competent blocks ranging from boulders to large slide blocks of strata >1 km in diameter, sometimes within a muddy, easily compactible debris-flow matrix (Alves & Cartwright, 2010; Armitage, Romans, Covault, & Graham, 2009; Hampton, Lee, & Locat, 1996; Masson et al., 2006; Pickering & Corregidor, 2005; Posamentier & Kolla, 2003). When containing large slide blocks thicker than the deposit, mass-transport deposits can generate topographic highs on the seafloor that enhance its roughness (Alves, 2010; Armitage et al., 2009).

Subsequently, submarine channels and turbidity currents can be confined by these same unburied slide blocks (Alves, 2010; Gamboa et al., 2010; McAdoo, Capone, & Minder, 2004; Pickering & Corregidor, 2005).

Lithological differences between slide blocks and surrounding strata can have a marked effect on the sea floor. After the blocks are completely buried by sediment, they can influence the degree of compaction of slope strata and, therefore, seafloor sediment distribution during early burial (Alves & Cartwright, 2010). Variations in compaction rate (differential compaction) can produce local topographic highs above the less compactible strata and increase accommodation space over the more compactible units (Hunt & Swarbrick, 1996; Maillard, Gaullier, Vendeville, & Odonne, 2003; Rusciadelli & Di Simone, 2007). Such a phenomenon has a profound effect on the subsequent architecture of slope sediment; differential compaction over mud-rich deposits can lead to the development of both local and regional depocentres (Dykstra et al., 2011). In addition, compaction processes can induce important slope instability (Bjørlykke & Høeg, 1997; Dugan & Flemings, 2000; Stigall & Dugan, 2010).

In the study area, differential compaction is observed over competent slide blocks that constitute part of a Late Miocene mass-transport deposit (MTD A) that was triggered in association with gentle folding and faulting of the Espírito Santo continental slope (SE Brazil; Figure 1). A newly identified sediment fairway and its relationship with slide blocks in MTD A was analysed. Also discussed is the development of linear depocentres over MTD A. Statistical analyses were used to recognize any scaling relationships between stratigraphic features in the study area. Hence, this paper addresses the following research questions:

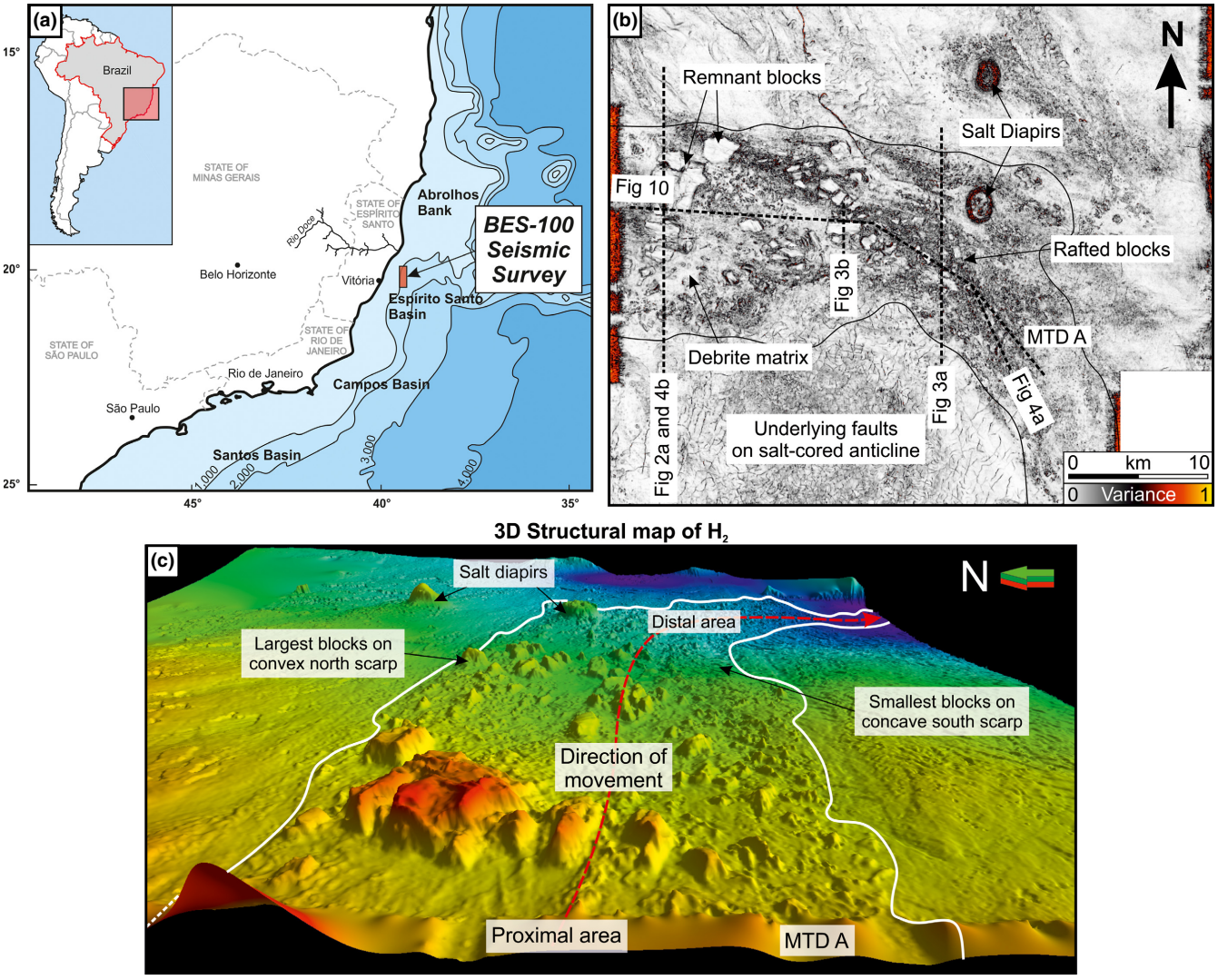

FIGURE 1 (a) Map of SE Brazil highlighting the location of the interpreted 3D seismic block in the Espírito Santo Basin. This sedimentary basin is situated between the Campos Basin to the south and the Abrolhos Bank to the north. (b) Variance cube of the studied MTD A as flattened at its base to show all relevant morphological features on the continental slope, and includes the boundary of MTD A (adapted from Alves & Cartwright, 2010). (c) 3D window view of a map of horizon H_2, the top of MTD A. It highlights the direction of flow downslope

1. What process created seafloor depocentres after MTD A was buried?
2. How did MTD A control the seafloor sediment distribution post-burial?
3. What constraints do the slide blocks impose on the size and scale of overlying stratigraphic features?

New isochron maps, structural maps and statistical data are presented to try to understand the relationship between MTD blocks and sediment distribution in younger strata offshore Espírito Santo. The impact of differential compaction on seafloor roughness is later discussed, focussing on the implications for submarine channel systems on continental slopes.

2 | DATA AND METHODS

The three-dimensional (3D) seismic volume used in this study (BES-100) covers an area of 2,450 km^2 on the mid-continental slope of Espírito Santo, offshore Brazil (Figure 1a). The interpreted zero-phased migrated volume was acquired using a dual airgun array and six 5,700 m-long streamers, and later processed within a 12.5 m × 12.5 m bin grid. Data were sampled every 2 ms following inline and cross-line spacings of 12.5 m. Data processing included data resampling at 4 ms, amplitude recovery, anti-aliasing filtering, time-variant filtering and predictive deconvolution, prior to stacking and 3D prestack time migration using the full Kirchoff algorithm. All time-depth conversions used an estimated seismic velocity of 1,800 m/s TWTT. Main seismic-stratigraphic units were identified using published well data from the Deep-Sea Drilling Project (DSDP) Sites 356 (Kumar, Gamboa, Schreiber, & Mascle, 1977) and 515/516 (Barker, 1983; Barker, Buffler, & Gambôa, 1983), and the work of Alves, Cartwright, and Davies (2009), Chang, Kowsmann, Figueiredo, and Bender (1992), Fiduk, Brush, Anderson, Gibbs, and Rowan (2004), Gamboa and Alves (2015b), Meisling, Cobbold, and Mount (2001) and Viana et al. (2003).

This study focussed on the strata overlying MTD A. Five horizons were mapped and analysed between the base of MTD A and the seafloor (e.g. Figures 1c and 2). The upper and lower surfaces of mass-transport deposits are

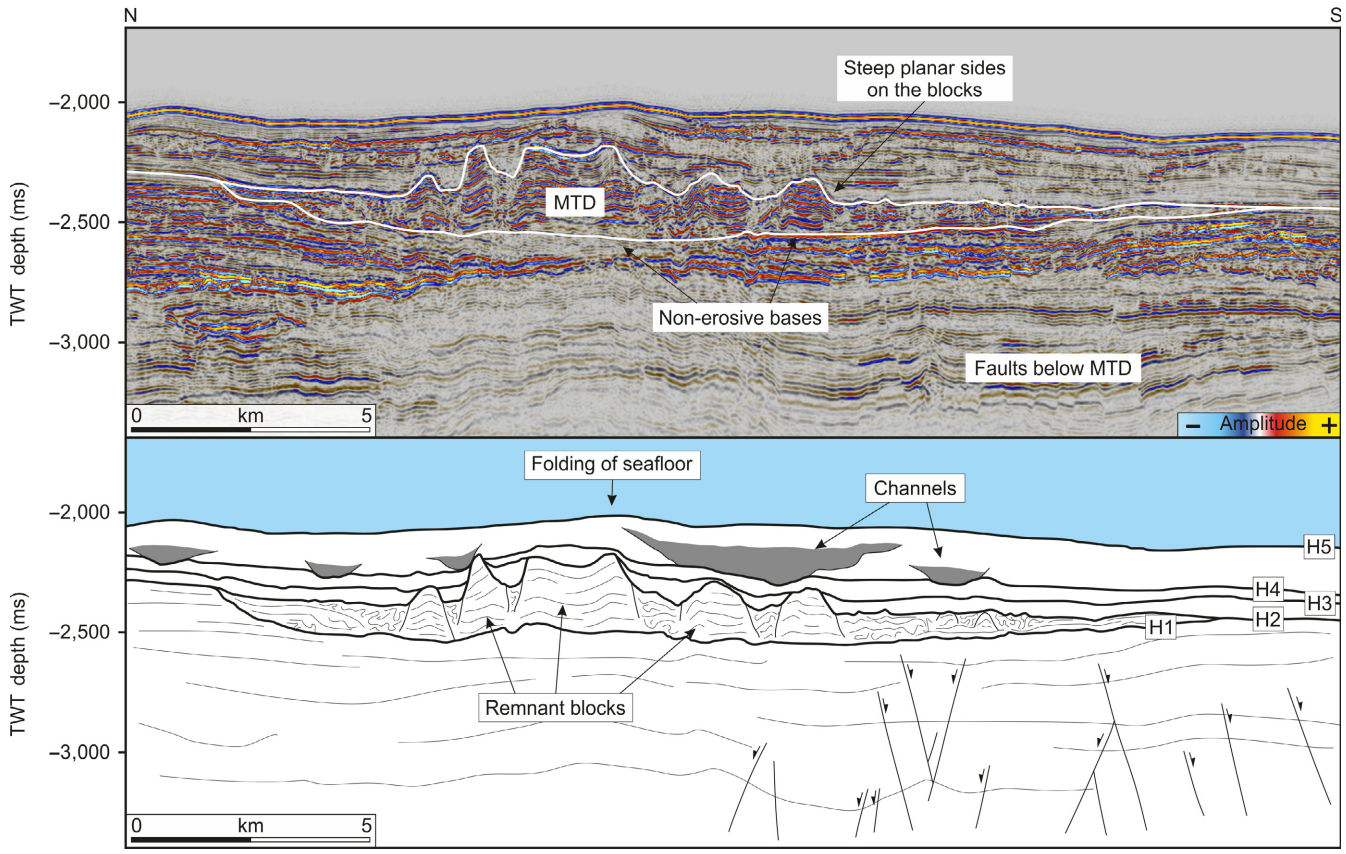

FIGURE 2 Selected N-S seismic section through the largest blocks in the studied MTD. Below is an interpretation of the seismic section. The key features studied include remnant blocks, channels and folds over the MTD. Also highlighted are the interpreted seismic horizons (H_1–H_5). These represent: H_1—the base of MTD A; H_2—the top of MTD A; H_3—moderately transparent reflections signalling a healing seafloor; H_4—overburden affected by differential compaction over the small blocks; H_5—present day seafloor. Location in Figure 1b

often irregular, which can lead to oversimplified structural maps being produced (e.g. Alves, 2010). The picking accuracy is also hindered by terminations and limited continuity of seismic reflections within discrete sedimentary packages (Figure 3). Detailed mapping was of vital importance to this study; structural maps for H_1, H_2 and H_4 were created using every inline and crossline, i.e. interpreted every 12.5 m. Consequently, metre-scale features were documented along the base of slope depocentres and channels, and the top surfaces of the MTD blocks were imaged at a resolution of <10 m (Figure 1c).

Variance data enabled us to investigate key structural and stratigraphic features on seismic data (Figure 1b). As the studied continental slope dips to the SE, the entire seismic cube was flattened to the base of MTD A (H_1) so that variance slices could be extracted through its full length. Isochron maps were also computed between the interpreted seismic horizons, a procedure that allowed us to visually compare features in MTD A with those of strata above it. Statistical data on imaged depocentres and slide blocks were compiled using direct measurements on vertical seismic profiles, converted to depth using an estimated seismic velocity of 1,800 m/s.

Width:height ratios were calculated to compute scaling relationships in depocentres and channels. Slide blocks were analysed by measuring their average width in plan view, and their height was recorded as the relief above debrites, i.e. from H_2 (top debrites) to the top of the block. Channel width was measured perpendicularly to its axis, and channel height was measured from the base of the channel to the top of the channel fill. Depocentres, represented on the plots as described in section 5.1, were measured similar to the channels. As they lie perpendicular to the flow direction, width represents the depocentres' short axes. Only the linear-elliptical depocentres that formed in the distal parts of MTD A were measured for the width: height plots. In total, the width and height of 56 depocentres, 81 blocks and 28 channels were measured and their ratios calculated (see Table S1).

3 | GEOLOGICAL SETTING

The Espírito Santo Basin is situated on the continental slope of SE Brazil. It is bounded by the Abrolhos Bank to the north and the Campos Basin to the south (Figure 1a).

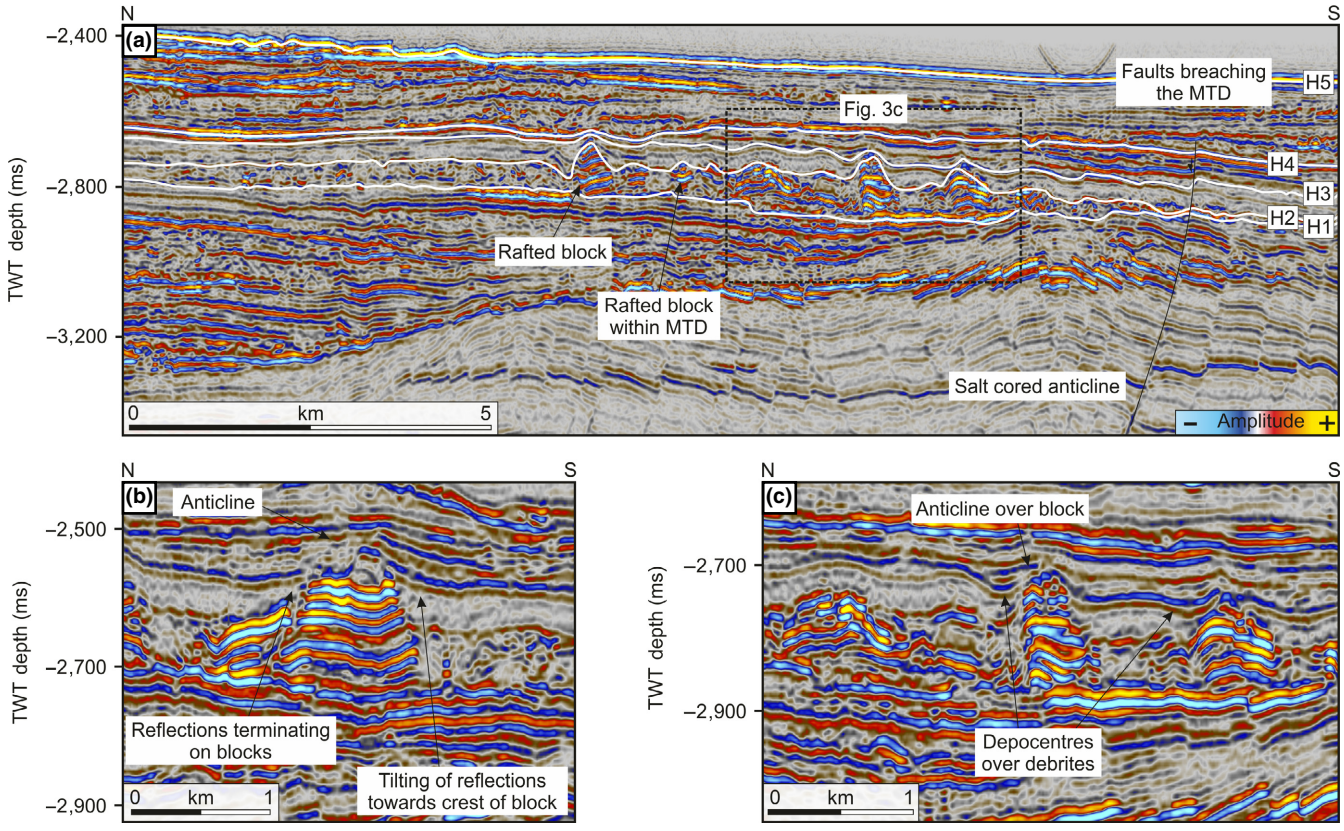

FIGURE 3 (a) Seismic profile crossing the rafted blocks in MTD A. From this seismic section, the "ripple-like" morphology of the overburden indicates where the depocentres are. Faults lying atop the salt-cored anticline are shown below the MTD. (b) and (c) are close ups of the remnant and rafted blocks shown in Figures 2 and 3a. (b) A large remnant block is surrounded by debrites. These debrites tilt towards the crest of the block, an indication of differential compaction. (c) Rafted blocks with depocentres forming between them, located over the debrites. Small anticlines over the blocks (as seen in Figure 3a) are also a sign of differential compaction. Location in Figure 1b

The basin developed from the Late Jurassic to Cretaceous, coevally with the opening of the South Atlantic (Chang et al., 1992; Davison, 1999; Fiduk et al., 2004). The oldest strata in the basin were deposited during the syn-rift phase (Late Berriasian to Early Aptian). It consists of continental sandstones, syn-tectonic conglomerates and igneous material (Chang et al., 1992; Fiduk et al., 2004; Mohriak, Nemčok, & Enciso, 2008; Ojeda, 1982). Tectonic quiescence during the transitional phase (Early Aptian to Late Aptian/Early Albian) led to the deposition of clastic, carbonate and thick evaporite sequences (Demercian, Szatmari, & Cobbold, 1993; Mohriak et al., 2008; Ojeda, 1982). The drift phase comprises two main depositional megasequences (Fiduk et al., 2004). The early drift is characterized by a transgressive shallow water carbonate platform buried by marls and shales that are indicative of basin deepening (Chang et al., 1992; Demercian et al., 1993). The late drift is separated from the early drift by a major unconformity. Clastic sediment was, at this stage, derived from the erosion of coastal mountain ranges and volcanic activity in the Abrolhos Bank (Chang et al., 1992; Fiduk et al., 2004).

Sediment transport occurred on Brazil's eastern margin since the Early Cenozoic, concentrated in the Upper Oligocene to Holocene channel systems (Alves, 2010; Fiduk et al., 2004; Viana et al., 2003). At least eight episodes of submarine-canyon incision and mass-wasting have occurred in the Espírito Santo Basin since the Late Cretaceous (Fiduk et al., 2004). Between the Early/Mid Eocene and the Holocene, MTDs were deposited in response to the uplift of coastal mountain ranges, local slope oversteepening and halokinesis (Alves & Cartwright, 2010; Mohriak et al., 2008). Cenozoic successions, including MTD A, comprise sediment aggraded during transgressive and highstand system tracts, and prograding strata associated with regressive episodes and submarine-canyon incision (Alves, 2010; Fiduk et al., 2004). Mud-rich depositional tracts (shelf-margin deltas and hemipelagic wedges) deposited in highstand and transgressive periods alternate with gravitational and sandy depositional tracts (canyons, deltas and meandering channels) accumulated during lowstand periods (Alves, 2010). The studied MTD A is thought to have been deposited during a Late Miocene regressive episode (Alves & Cartwright, 2010; Alves et al., 2009; Mohriak et al., 2008). Competent remnant and rafted blocks within MTD A are part of the Caravelas Formation, which was deposited on a carbonate shelf from the late Eocene (Bartonian) onwards (Alves, Kurtev, Moore, & Strasser, 2014; Asmus, Gomes, & Pereira, 1971; Fiduk et al., 2004; Mohriak et al., 2008). The modern continental slope comprises turbidites, calcarenites and calcareous mudstones, and overlies Early Cenozoic carbonates and shales belonging to the Early Urucutuca and Regência Formations (Alves & Cartwright, 2010; Mohriak et al., 2008).

Progradation of strata onto the continental slope promoted significant halokinesis due to the differential loading of thick Aptian evaporites (Fiduk et al., 2004). The downslope movement of salt fed salt anticlines, salt rollers and vertical salt diapirs (Alves & Cartwright, 2010; Davison, 2007). Most of the salt growth in the basin occurred after the Albian, but peaked in the Late Cenozoic (Fiduk et al., 2004; Mohriak et al., 2008). On the upper continental slope, halokinesis occurred in parallel with thin-skinned extension, which was triggered by gravitational gliding over Aptian evaporites (Demercian et al., 1993). Gravitational collapse of salt-cored anticlines led to the formation of extensional faults (Alves, 2010; Alves et al., 2009; Baudon & Cartwright, 2008). These crestal and axial fault sets are associated with peaks in halokinesis, but have also experienced younger reactivation (Baudon & Cartwright, 2008). The vertical propagation of faults during reactivation controlled the geometry of remnant blocks in the studied MTD A. The base of this same deposit shows multiple types of faults above salt anticlines, rollers and diapirs (Alves, 2010).

4 | SEISMIC STRATIGRAPHY

4.1 | MTD A (H_1–H_3)

MTD A is characterized by coherent and moderately deformed remnant blocks (Figure 2). Highly deformed (rafted) blocks are also observed in debris-flow deposits, or debrites (Figure 3a). Using the classification scheme of Moscardelli and Wood (2008), the MTD has been interpreted as a "slope-attached MTD". Its surface area is ~440 km^2, it has a maximum width of <16 km and is ~40 km in length. The length:width ratio of the MTD is >2. The headwall of MTD A is not imaged on the seismic data. However, the presence of remnant blocks exceeding 5 km width in the proximal part of MTD A indicates the proximity of the headwall to the west of the study area. The largest blocks, both remnant and rafted, occupy the convex north scarp of MTD A, decreasing in size towards its concave south scarp (Figure 1b, c). This distribution also occurs from the proximal region to the distal region; as a result, the largest blocks lie in the head of MTD A, decreasing in size towards its toe (Figure 1b).

Remnant blocks, which are in general the largest blocks, comprise parallel, sub-horizontal, high amplitude seismic reflections representing relatively undeformed slide blocks (Figure 3b). Their bases generally correlate with the base of MTD A (H_1), indicating they have experienced limited movement (Figure 2). These blocks can range from >5 km to <1 km in width, >200 ms (~180 m) height (from the base to the top) and commonly have steep, planar sides (Figure 3b). Conversely, rafted blocks are much smaller

than remnant blocks; they are <500 m wide and show a similar height to the MTD itself (<100 ms or ~90 m). Internal seismic reflections are also parallel, but are rotated and the blocks are normally suspended within debrites in MTD A (Figure 3c). Rafted blocks, therefore, were transported downslope during separate pulses of mass wasting, either sitting above previous debris flows, or having been covered by later debris flows during multiple failure events (Minisini, Trincardi, Asioli, Canu, & Foglini, 2007).

Based on their chaotic and relatively low amplitude character, strata between the blocks are interpreted as debrites (Figure 2). The top surface of the debrites is marked by a continuous seismic reflection. This indicates the cessation of the mass movement and the initiation of normal sediment fallout. The height of the debrite unit increases towards some of the largest blocks (Figure 3b).

Below MTD A, dense networks of faults deform a salt cored anticline (Figure 2). These were formed during halokinesis by gentle folding of post-salt strata during the Miocene (Alves & Cartwright, 2010; Omosanya & Alves, 2013). In the proximal part of the MTD, faults rarely breach H_1 (Figure 2). Downslope, the faults are closer to the surface and it is not uncommon for H_1 to be breached by vertically propagating faults, especially when MTD A is not present (Figure 3a).

4.2 | Overburden (H_3–H_5)

Once MTD A was emplaced, the seafloor began to heal. The topographic lows that formed over the debrites and between the blocks were filled with relatively homogenous sediment, displaying low amplitude and semi-continuous seismic reflections (Figure 3b). This low amplitude unit is <100 ms (~90 m) thick. It covers all of the smaller blocks, including all the rafted blocks in the distal part of MTD A, and is bounded by H_2 at its base and H_3 at its top (Figure 4). However, remnant blocks taller than this unit were not buried and maintained their topographic relief on the seafloor. Seismic reflections onlapped the sides of these exposed blocks and are folded upwards towards their crest (Figure 3b). In comparison, seismic reflections that are continuous over the smaller blocks in MTD A (i.e. having buried the blocks) are folded, creating small anticlines and depocentres (Figure 4a).

Overlying the healed seafloor is a unit ~200 to 300 ms thick that includes all the strata from the top of MTD A (H_3) to the seafloor (H_5). Seismic reflections in this interval vary from very high amplitude to low amplitude, and are chaotic to semi-continuous (Figure 4b). Very few seismic reflections are completely continuous in this unit, owing to the large number of channels and scours truncating them (Figure 4b). These erosional features are orientated in a similar direction to MTD A; N-S cross sections across MTD A display the typical lenticular shape of the channels (Figure 4a, b). Each reflection is a constant amplitude in the direction of movement (Figure 4a), but changes amplitude across the width of MTD A (Figure 4b).

5 | EVIDENCE OF DEFORMATION OVER MTD A

5.1 | Early differential compaction over and around slide blocks

Differential compaction during early burial tends to occur in association with variations in lithology, which impose unequal rates of mechanical compaction in strata (Trask, 1931; Weller, 1959). In the case of MTD A differential compaction is believed to have occurred over the blocks, i.e. under-consolidated debrites compacted more than relatively rigid carbonate blocks. This process therefore led to forced folding of strata over MTD A. Seismic reflection H_3 is continuous over the buried blocks and has a constant thickness (Figure 3a). Topographic highs developed along this horizon over the slide blocks, and local depocentres formed over the debrites, flanking the slide blocks (Figure 3c). The depocentres were filled with sub-horizontal reflections, onlapping their inside walls.

As previously described, the largest blocks maintained their topographic relief on the seafloor after the deposition of H_3, and in some cases H_4 (Figure 2a). However, gentle folds are also observed over these blocks, although channels eroded a large proportion of the fold limbs, making the identification of their true shape difficult (Figure 4b). The smaller anticlines and depocentres (~1 km wide, ~30 ms thick) do not continue above H_4, as seismic reflections become flat. The larger anticlines in the proximal part of MTD A (<5 km wide, ~100 ms thick) continue upwards over H4 influencing the shape of the present day seafloor (Figure 4b).

5.2 | Sediment fairways over MTD A

Channels and scours predominate in the complex strata overlying MTD A (Figure 5). Most are hard to distinguish from the surrounding material: they are low amplitude and filled with parallel horizontal seismic reflections, which are truncated on the inner channel walls (Figure 4b). Other channels have slightly chaotic fill, which could be indicative of mass flows (Figure 4b). They range from <1 km to more than >3 km wide and are situated above the debrites, always marginal to the large blocks and seldom eroding horizon H_3. These channels differ from the depocentres that are observed over the distal parts of MTD A because they are orientated parallel to the direction of movement of the latter deposit (Figure 5a).

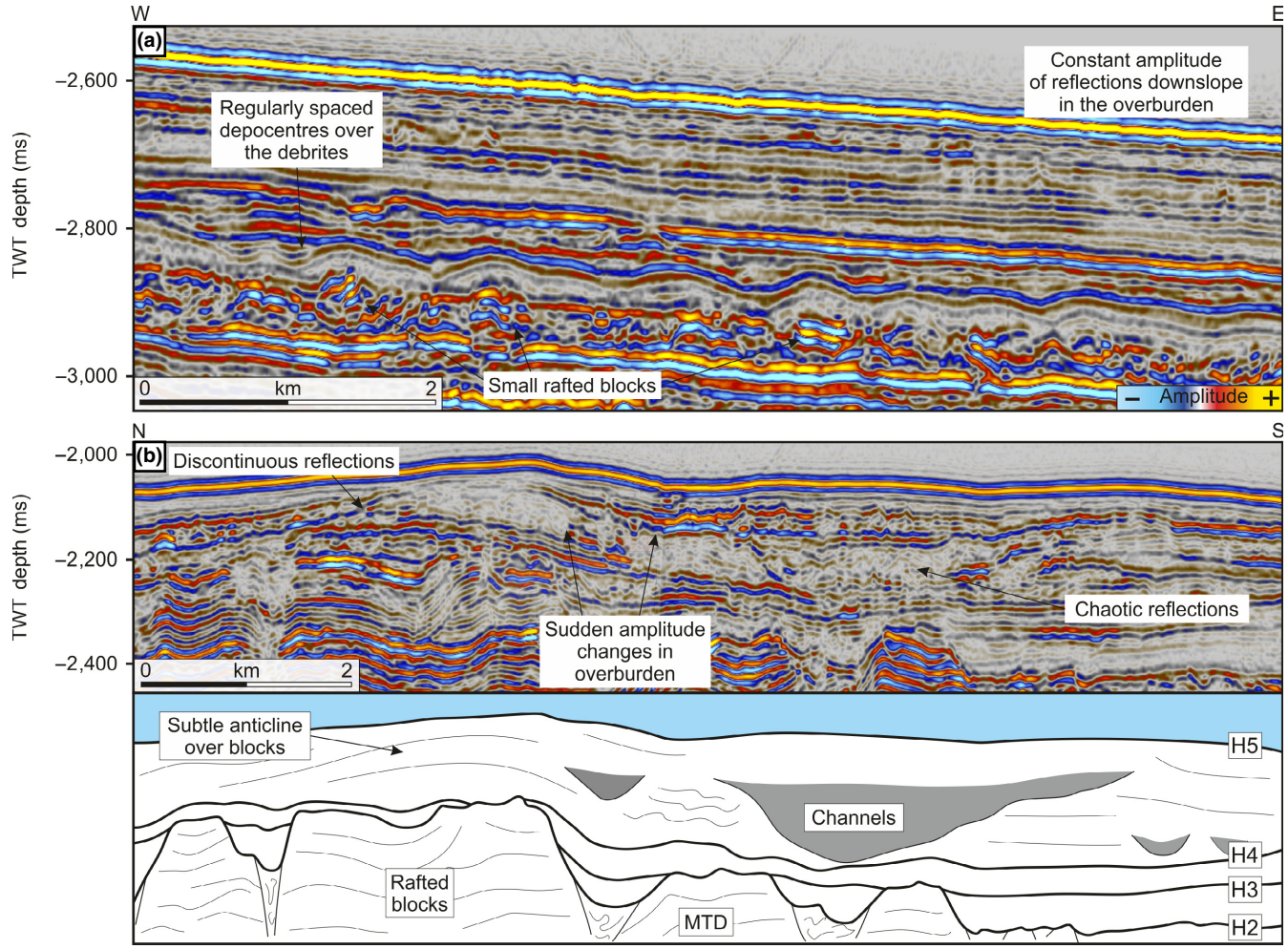

FIGURE 4 Seismic profiles of the strata overlying MTD A. (a) A downslope seismic section showing regularly spaced depocentres formed over small rafted blocks entrained within the debrite matrix. The reflections downslope also have a relatively constant amplitude. (b) Seismic section perpendicular to the flow direction, highlighting the channels in the overburden, as well as the seismic characteristics. There are lots of discontinuous reflections as the channels have eroded into the overburden. The reflections range from chaotic-continuous and transparent-opaque. It is hard to pick out features of deformation in the overburden because of the complexity of seismic facies. Location in Figure 1b

A TWT structural map of H_3 shows a series of elongated striations striking downslope (Figure 5). This cluster of striations reaches a maximum width of 2.5 km, and they are continuous for at least 25 km (Figure 5a). At its greatest width, there are up to 12 striations side by side in the observed cluster. Towards the termination of the striations, the shape resembles that of a submarine fan as they splay out, almost doubling the width of the cluster (Figure 5b). Striations similar in size and geometry to those studied here are commonly associated with glacial movements (Rise, Olesen, Rokoengen, Ottesen, & Riis, 2004; Dowdeswell, Ottesen, Rise, & Craig, 2007), the base of submarine landslides (Gee, Gawthorpe, & Friedmann, 2005), precursors to submarine channels (Gee, Gawthorpe, Bakke, & Friedmann, 2007) or below debris flows (Posamentier & Kolla, 2003). Directly above the striations lies a channel system (Figure 6). It remains unclear whether the striations were formed during the early growth of the channel, or if MTD processes created them, and the channel infilled the newly created space. Regardless of the timing, the channel is evidence for incision in the areas that lack large slide blocks.

6 | SCALING RELATIONSHIPS BETWEEN SLOPE STRATIGRAPHIC ELEMENTS

Statistical analyses were undertaken to record the scaling relationships between width and height of different stratigraphic elements, in the case of depocentres, channels and blocks associated with MTD A (see Table S1; Gamboa & Alves, 2015a). Log-log plots were used to compare the width:height ratio between each of the elements (Figures 7 and 8). Width:height ratios of the blocks range from three (3) to 15, and the mean is eight (8) (Figure 7a). Most of the blocks lie within a dense cluster of ratios varying from

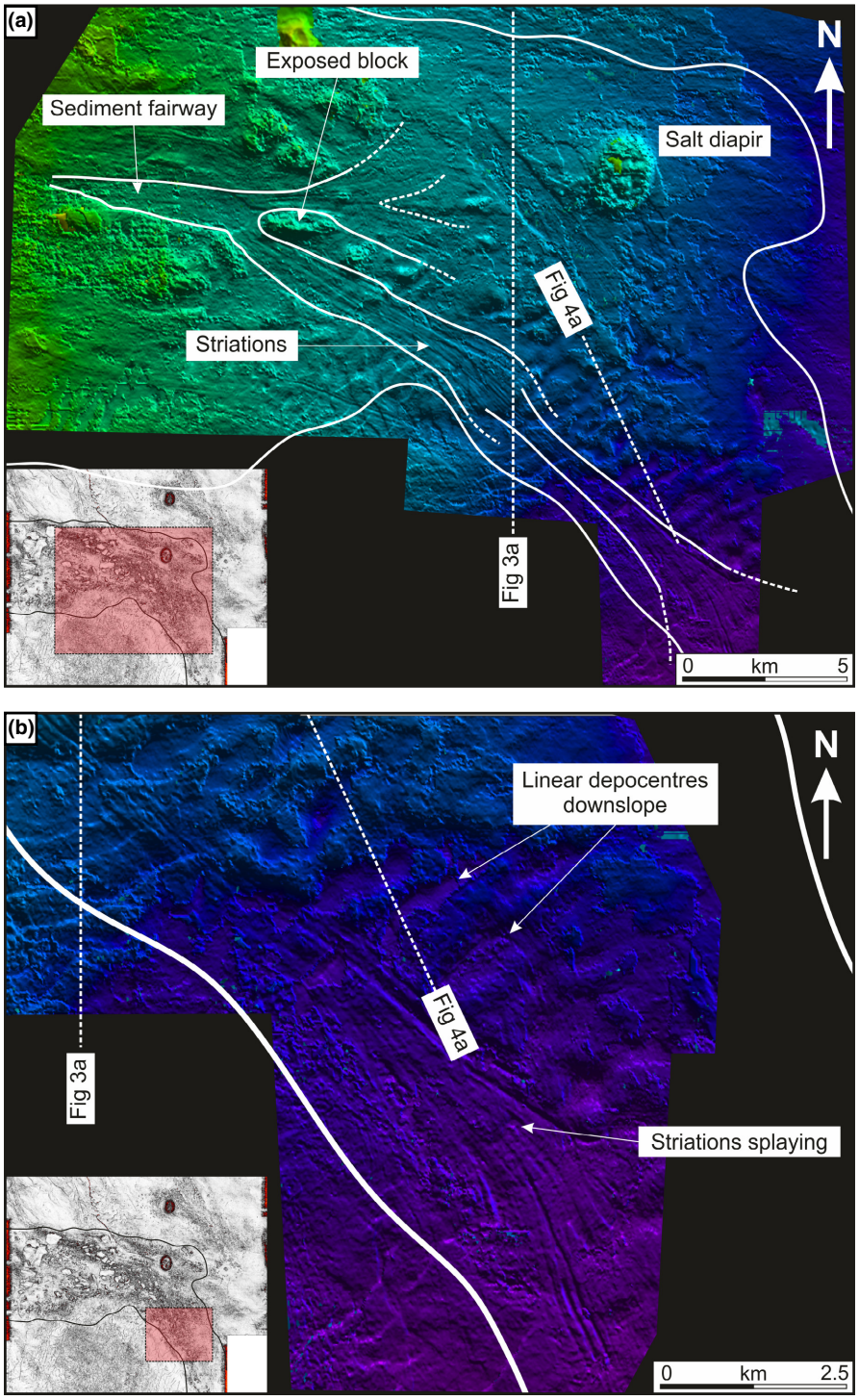

FIGURE 5 (a) TWT structural map of H_3 giving an overview of the sediment fairway. The boundary of MTD A is shown in white. The striated fairway appears to have moved downslope, along the margin of MTD A. An exposed block disrupts the pathway of the fairway, bifurcating it near the origin. (b) Close up of the striations downslope (location shown on the map within the figure). The striations have a fan shape at the terminus. The fairway cuts through elliptical-linear depocentres, observed on the NE side of it

6 to 10, as the standard deviation is two (2). The minimum and maximum ratios for the depocentres were seven (7) and 39, respectively, with a mean of 18 (Figure 7b). The standard deviation is six (6), so most of the depocentres lie within a ratio of 12–24. The submarine channels have higher width:height ratios, ranging from 17 to 30, with a mean of 23 and a standard deviation of 4 (Figure 7c). Figure 8a shows regions where values overlap in dark grey and similar ratios can be expected between channels and depocentres, and blocks and depocentres. Results show there is a linear scaling trend; the wider each element is, the taller it is expected to be. Although their trends are similar, there is an obvious decrease in width:height ratios when comparing the stratigraphic elements in the overburden (channels and depocentres), with those emplaced in MTD A (blocks; Figure 8a).

These results are compared with width and height measurements from different stratigraphic elements in the

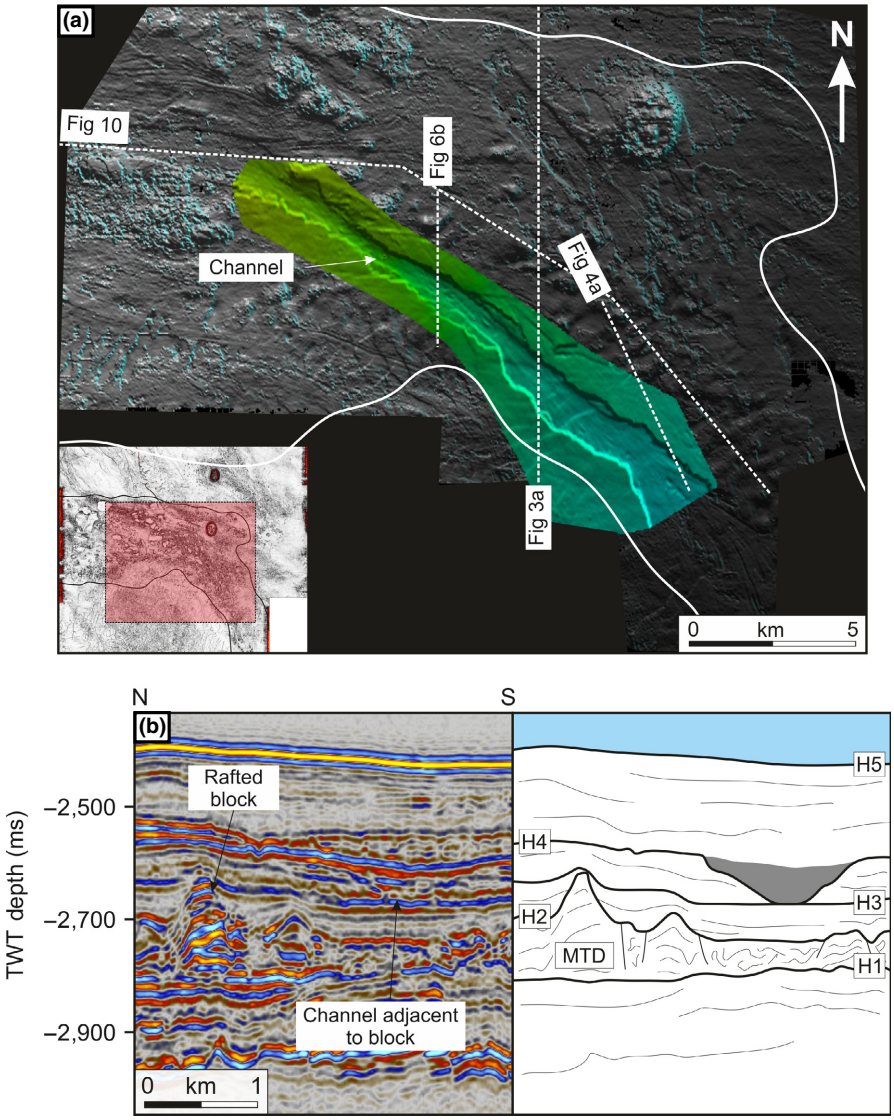

FIGURE 6 (a) TWT structural map of the main channel travelling directly over the striations observed on Figure 5a. The channel has a similar fan shape geometry at the terminus. The map of H_3 is included in grey, to help highlight the channel. (b) Seismic cross section through the channel and blocks lateral to it. An interpreted profile next to it highlights the key features. The channel is bound by H_3–H_4 and occurs directly over the debrites. A small anticline occurs along H_4 over the rafted block

literature. These include MTD blocks (Gamboa & Alves, 2015a; McHargue et al., 2011; Moscardelli & Wood, 2008; Omosanya & Alves, 2014), different elements from within a channel system (Babonneau, Savoye, Cremer, & Klein, 2002; Clark & Pickering, 1996; Deptuck, Sylvester, Pirmez, & O'Byrne, 2007; Di Celma, Brunt, Hodgson, Flint, & Kavanagh, 2011; Gamboa & Alves, 2015a; Gong et al., 2016; Qin, Alves, Constantine, & Gamboa, 2017), landslides, debris flows and MTDs (Gamboa & Alves, 2015a; Hampton et al., 1996; Masson et al., 2006) and plunge pools (Lee, Talling, Ernst, & Hogg, 2002). All these data are compiled on a graph (Figure 8b). The data include 140 measurements, ranging from scales of 10s of metres to 10s of kilometres, and there is a high density of measurements within the boundaries of those from this study. Scaling trends observed in data from this study are consistent with stratigraphic elements from literature. Mass-transport deposits and landslides occupy the lower width:height ratios, whereas channel elements have larger width:height values (Figure 8b). The blocks show a wider range in width:height values, though all are greater than the ones in MTD A. Strikingly, nearly all the data on the graph fall within width:height ratios between 5 and 35. This suggests that the scaling trend observed between blocks, channels and depocentres can be applied to a variety of other stratigraphic elements on continental margins. However, caution needs to be taken when comparing stratigraphic elements in different settings. Without knowing the stratigraphic and structural relationships between individual elements and completing detailed analyses of the features (as performed in this study), scaling trends would render meaningless.

Isochron maps were created for different units in this study area by Alves (2010); Alves and Cartwright (2010); Gamboa et al. (2010); Omosanya and Alves (2013); Gamboa and Alves (2016), but none of the maps produced have been high enough quality to resolve smaller features such as the linear depocentres on the margins of MTD A. Isochron maps were used to help understand the size,

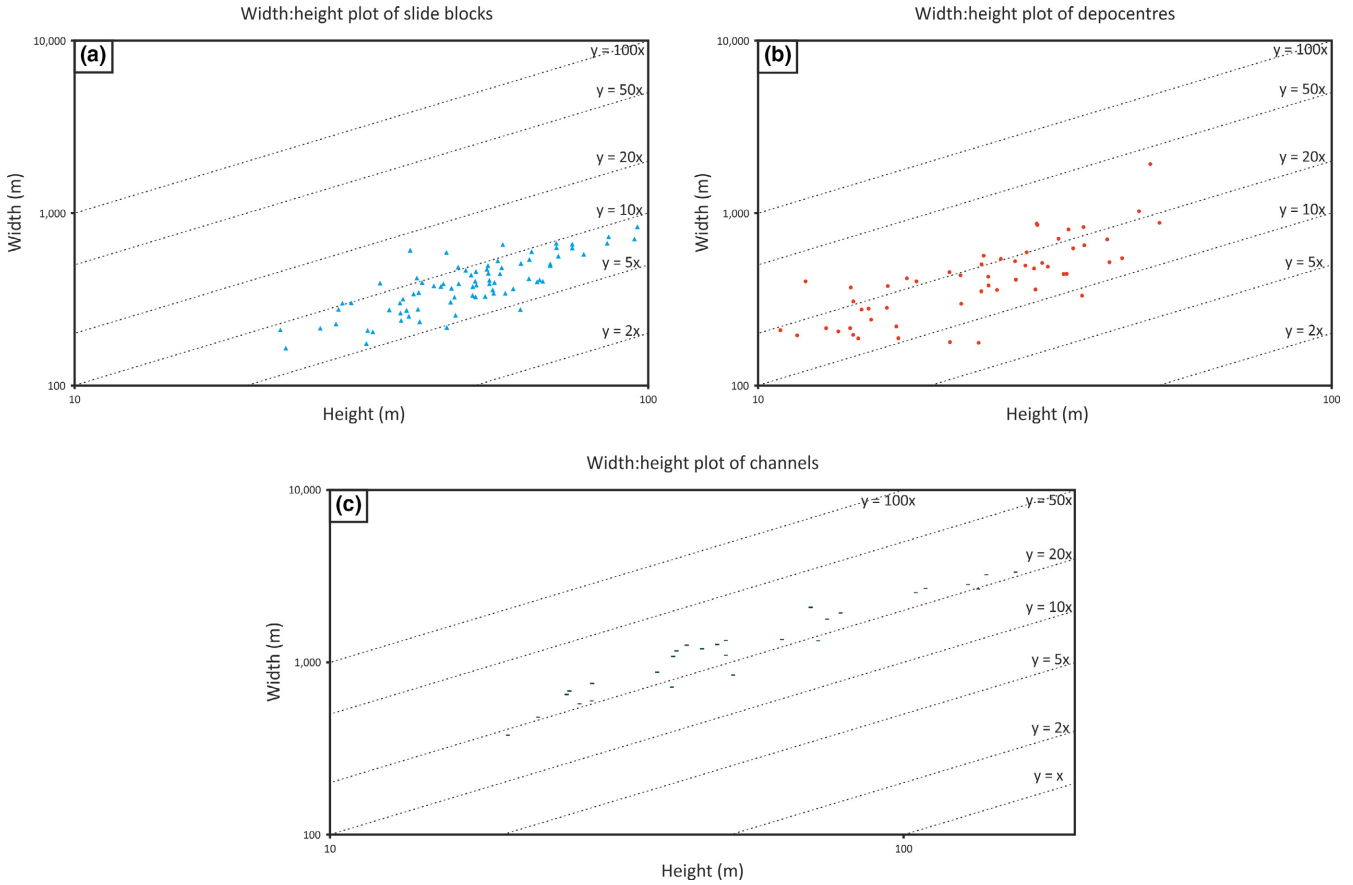

FIGURE 7 Log-log plots of the different stratigraphic elements in the study area. The width:height ratios are shown as dashed lines at regular intervals. The graphs are as follows: (a) blocks within MTD A; (b) depressions above MTD A, along horizon H4; (c) channels overlying MTD A

geometry and timing of creation of depocentres above this same MTD (Figure 9). Figure 9a represents the thickness between H_3 and H_4. It shows the linear depocentres that formed above H_3 along the southern margin and the distal parts of MTD A (Figure 9a). It also highlights the thickness increase downslope along the axis of MTD A. Post-MTD A deposition was concentrated above the MTD itself, away from the slide blocks. In similarity to Figure 9a, an increase in thickness downslope suggests accommodation space was still present after MTD A was buried by, at least, horizon H_4 (Figure 9b). Sediment fairways are displayed on the isochron map as dark purple, i.e. the thickest sediment packages (Figures 6 and 9a). These are relatively linear features orientated along the flow direction of MTD A. Each channel overlies the debrites and flowed through the chasms between blocks. Blocks that were still exposed on the seafloor at the time of H_4 deposition are red. Blocks highlighted in yellow were buried and structural relief over them was created by differential compaction.

Figure 9b is an overlay of two separate maps: (a) TWT structural map of the seafloor, (b) an isochron map of the overburden (H_2–H_5). Blocks within MTD A are easily identifiable because they were positive topographic features and have less strata overlying them than surrounding debrites. The boundaries of MTD A correlate with a thicker sediment package in the overburden (red colour). This represents the folding of the seafloor over MTD A (Figure 2). One final feature of interest is the location of a channel on the present day seafloor over MTD A (Figure 9b). The anticline has created an irregular seafloor, causing the channel to form along its axis. Similar to the channel investigated in Figure 6, this one flows between the largest blocks and over the debrites. Therefore, the blocks are still impacting the distribution of sediments on the present day seafloor.

7 | DISCUSSION

7.1 | Processes generating seafloor depocentres offshore Espírito Santo

The results obtained from seismic interpretation show a relationship between blocks within the MTD and overlying depocentres. As previously suggested, only those blocks that were positive relief structures after emplacement have anticlines situated over them, flanked on each side by

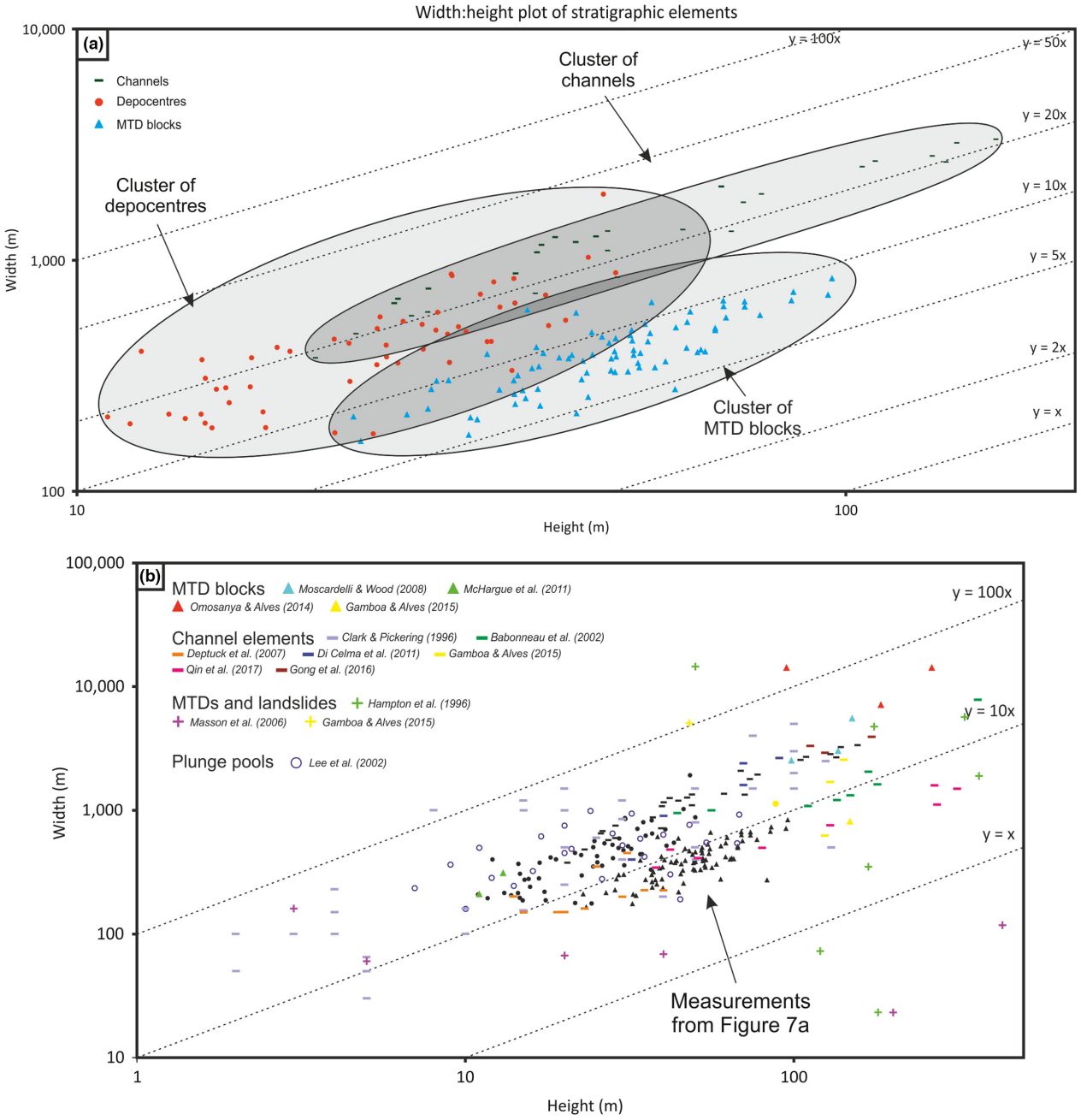

FIGURE 8 (a) A compilation of the log-log plots of each stratigraphic element in Figure 7. Ellipses have been drawn around all of the measurements for each separate feature (MTD block, depocentre and channel). The dark grey regions where they overlap are areas with similar ratios for different elements. All follow a similar trend line, but have increasing width:height ratios from the blocks, to depocentres, to channels. (b) Width:height plots comparing stratigraphic elements observed in this study and previous publications (Babonneau et al., 2002; Clark & Pickering, 1996; Deptuck et al., 2007; Di Celma et al., 2011; Gamboa & Alves, 2015a,b; Gong et al., 2016; Hampton et al., 1996; Masson et al., 2006; McHargue et al., 2011; Omosanya & Alves, 2014; Qin et al., 2017). The measurements from this study are black

depocentres. This is evidence for the control of the blocks within the MTD on the evolution and spatial distribution of depocentres. As the seafloor healed, accommodation space between the blocks was reduced (Armitage et al., 2009; Kneller, Dykstra, Fairweather, & Milana, 2016; Prather, 2003; Shultz, Fildani, Cope, & Graham, 2005). The blocks were subsequently buried. Timing of burial is directly related to the size of blocks and position on the slope. Smaller blocks at the toe of the MTD (downslope) were completely buried before H_3 was deposited (Figure 10), whereas larger blocks in the proximal region of MTD A (upslope) still had topographic relief until after the deposition of H_4 (Figure 10). This difference in timing could become an important control on the compaction history, as smaller blocks

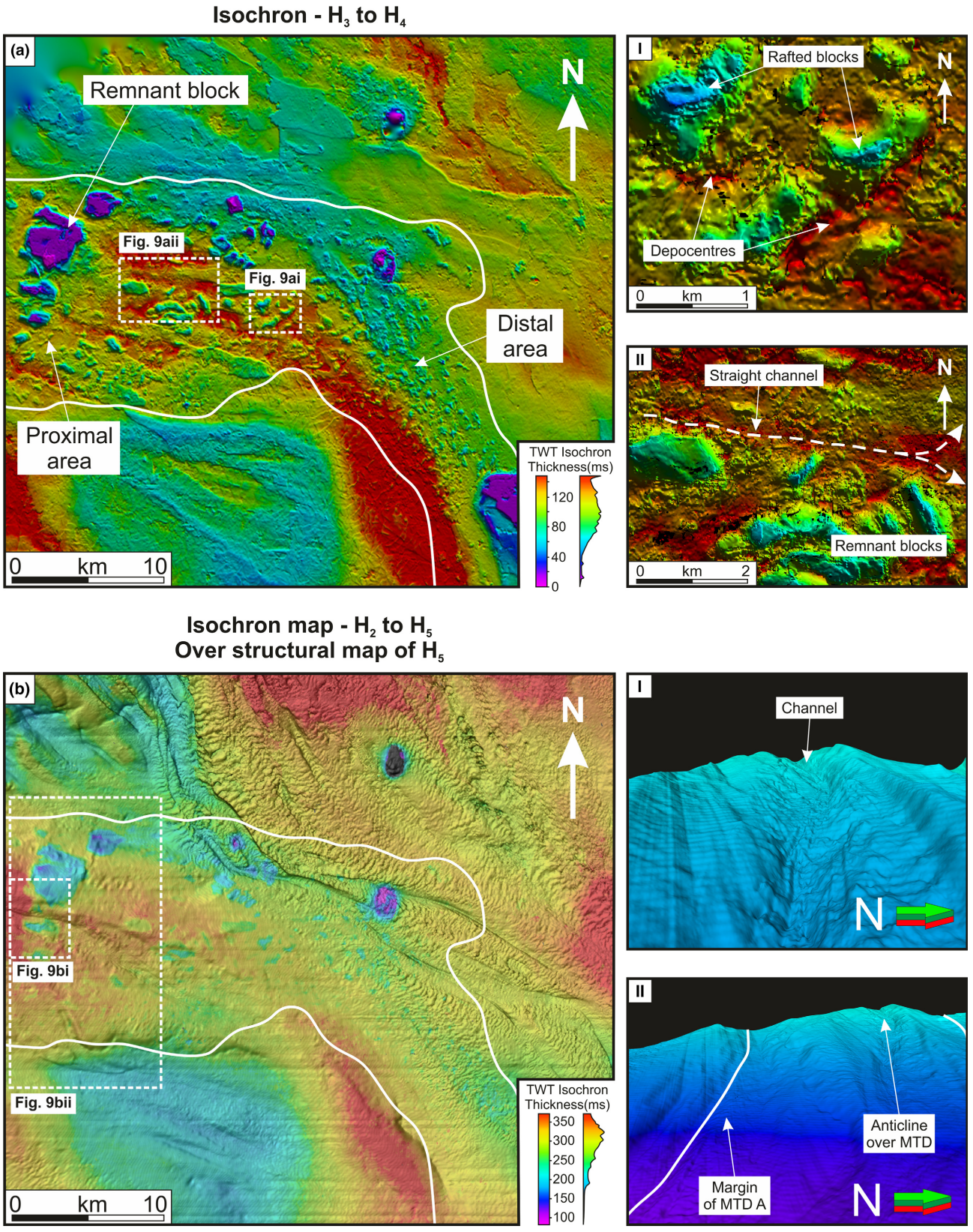

FIGURE 9 (a) Isochron map between H_3 and H_4 projected onto horizon H_3. The key characteristics are highlighted in ai and aii: (i) the depocentres and ridges formed over rafted blocks; (ii) channel in the overburden. (b) An isochron map of H_2 to H_5, overlain with a structural map of the seafloor. This map shows the thickness of the overburden relative to MTD A, and shows the features on the present day seafloor that resulted from differential compaction on a 3D interpreted horizon of the seafloor: (i) channel over the axis of MTD A, flowing over a chasm between blocks; (ii) anticline formed over MTD A

within the same mass-transport deposit will have undergone differential compaction before the largest blocks.

Near the headwall, the largest blocks in MTD A were still positive-relief structures until after the deposition of H_4 (Figure 10). Loading of the debrites between the blocks would cause them to start compacting before the blocks were buried. Evidence for this process can be seen in Figure 3b. Horizon H_3 is the top of the healed stratal package between the blocks and onlaps the sloping edge of a large block. This horizon is tilted towards the top surface of the block, due to the compaction of debrites (Figure 3b). This same geometry is replicated in the seismic reflections above H_3. Subtle anticlines fold over the top of these blocks, dipping towards the accommodation space created by the compacting debrites on both sides. The creation of accommodation space from differential compaction enhanced the size of depocentres over the debrites, even after the blocks were completely buried.

In the distal parts of MTD A, the blocks were completely buried with >50 ms (45 m) of sediment prior to the deposition of H_3 (Figure 3a). Continuous seismic reflections over the MTD in this area corroborate this interpretation. Here, the seafloor had completely healed prior to compaction (Armitage et al., 2009). However, as seen in the seismic data (Figure 3c) and the structural map of H_3 (Figure 11a), there are elliptical depocentres spaced at regular intervals in the strata immediately above the blocks (H_3–H_4). Two geological features may explain the evolution of the depocentres that dominate the distal part of MTD A: (a) smaller rafted blocks that rise above the debrites (Figure 11b) and (b) faults related to the underlying salt structures (Figure 11c). The faults in this region deform rocks below MTD A, rarely displacing strata above H_1. This has been attributed to the upper tip of the faults being eroded as MTD A was emplaced (Alves et al., 2009; Omosanya & Alves, 2013). Were the faults to propagate through MTD A, the depocentres could be linked to fault-related folds as there are mechanical contrasts between the MTD and its cover (Hardy & McClay, 1999). However, there is an obvious orientation to these structures, and fault scarps are easily discernible. These fault scarps occur south east of the margins of MTD A (Figure 11a). In contrast, the plan view geometry of depocentres is much more elliptical than the fault-related folds and they are also symmetrical in cross section (Figure 11). Between each of the depocentres there are a series of small rafted blocks. Horizon H_3 folds over the top of these blocks, creating gentle anticlines (Figure 11a).

Because of the continuous seismic reflections over the blocks and the spatial relationship between the blocks and depocentres, it is thought that the depocentres were enhanced (if not formed) by differential compaction: a larger load over the debrites led to greater compaction than the relatively small load over the rigid carbonate blocks. This work attributes the evolution of depocentres to differential compaction, but faults are known to produce similar features (Corfield & Sharp, 2000; Cosgrove & Ameen, 1999; Sharp, Gawthorpe, Underhill, & Gupta, 2000). It is therefore important to discuss the differences between the deformation caused by faults and differential compaction in this study, especially as the depocentres are relatively linear, evenly spaced features and orientated in the same direction as the underlying faults. Primarily, seismic reflections along H_3 deformed by the faults have distinctly different seismic characteristics to the depocentres formed over blocks in the same horizon. Most significantly, the faults create asymmetrical depocentres as the downthrown footwall rotates towards the fault scarp (Figure 11c). The depocentres over the blocks are symmetrical in cross section and the lowest point is directly above the debrites (Figure 11b). In addition, the hanging wall of some of the faults breaching H_1 lie beneath the middle of the

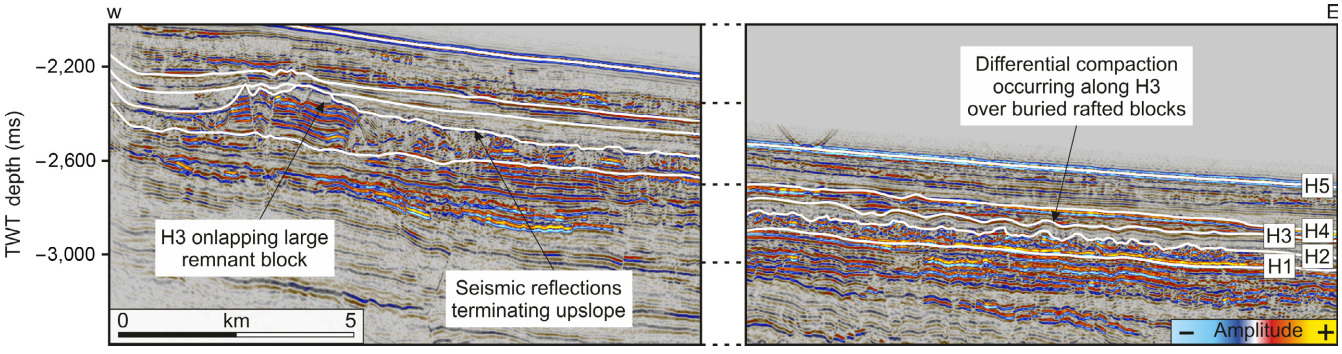

FIGURE 10 Downslope seismic section to show the differences between the overburden above large remnant blocks and smaller rafted blocks. Horizons in the proximal area (left box) are relatively parallel. Below H_4, they onlap the sides of the block, or terminate upslope onto MTD A. There was obviously increased topographic relief of MTD A whilst the overburden was being deposited. Downslope (right box), the reflections are folded over the rafted blocks along H_3, but return to almost flat when H_4 was deposited. This indicates differential compaction between the debrites and the blocks occurred early in burial. Location in Figure 6a

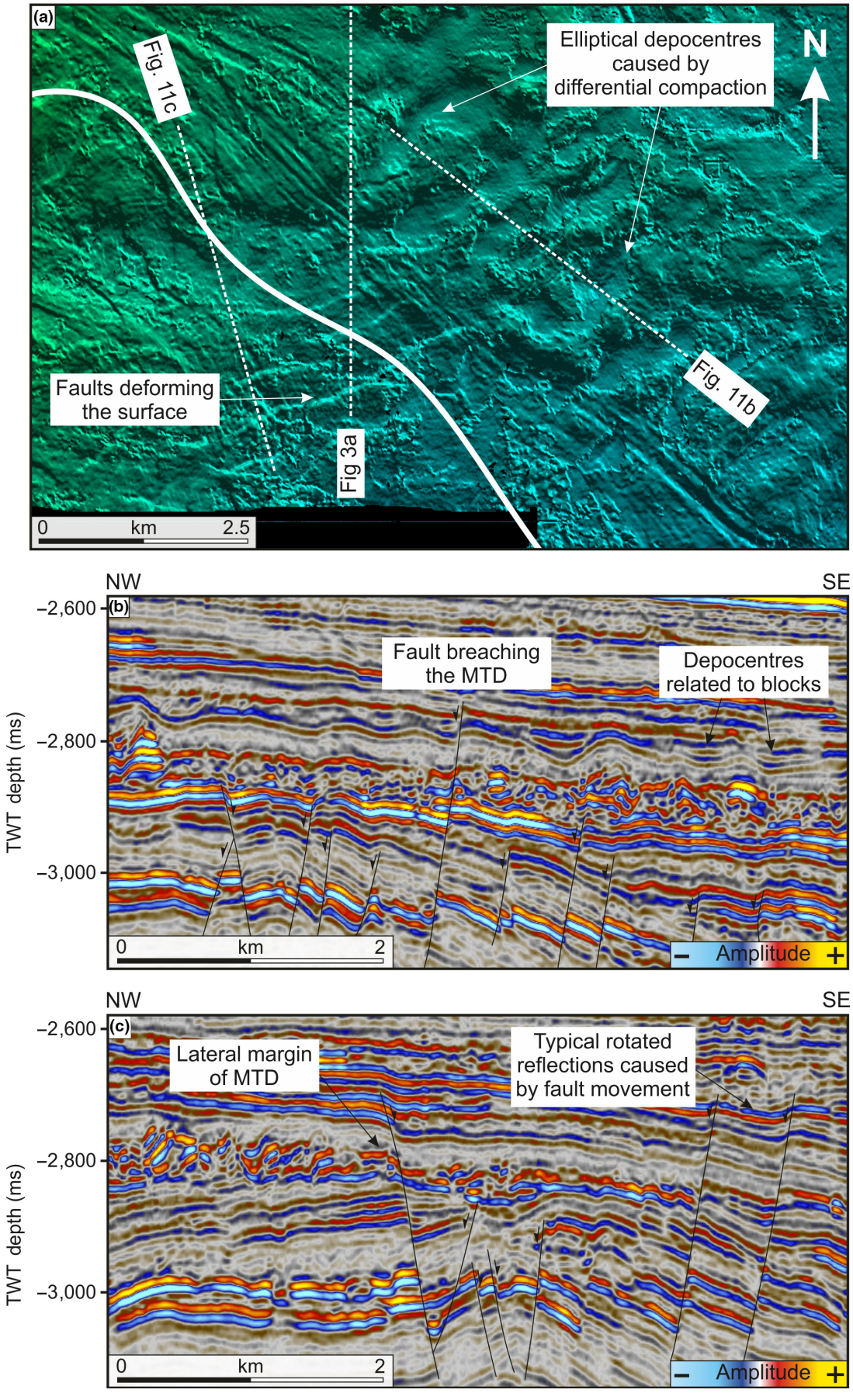
(a)
Fig. 11c
Elliptical depocentres caused by differential compaction
N
Fig. 11b
Faults deforming the surface
Fig 3a
0 km 2.5
NW
SE
(b)
−2,600
−2,800
−3,000
TWT depth (ms)
Fault breaching the MTD
Depocentres related to blocks
0 km 2
− Amplitude +
NW
SE
(c)
−2,600
−2,800
−3,000
TWT depth (ms)
Lateral margin of MTD
Typical rotated reflections caused by fault movement
0 km 2
− Amplitude +

FIGURE 11 (a) TWT structural map of H_3 taken from slightly further upslope than Figure 5b. The boundary of the MTD is represented by the white line. NW of the boundary (overlying the MTD), the seafloor has elliptical depocentres regularly spaced, lying perpendicular to the flow direction. In (b), the faults do not breach the MTD. It is therefore believed that these relatively symmetrical depocentres were influenced by differential compaction. A single fault passes through the MTD, giving the overburden the typical "rotated-block" style deformation expected by faults: the downthrown side rotates towards the fault surface. SW of the boundary (where the MTD pinches out), linear features are interpreted as fault movements. (c) A seismic line shows the faults deforming rocks where the MTD is not present

depocentres (Figure 11b). This contradicts the typical model of normal faults, where the hanging wall is up thrown. Also, the change in style between compaction-related depocentres and fault-related depocentres seems to be concurrent with the presence of MTD A, which prevents most faults from propagating through and above it (Figure 11).

7.2 | Impact of seafloor roughness created by MTD A

Once MTD A was emplaced, there were sharp topographic variations on the seafloor between the blocks and surrounding debrites. Some blocks protruded >50 m above the height of the debrites (Figure 2). This seafloor

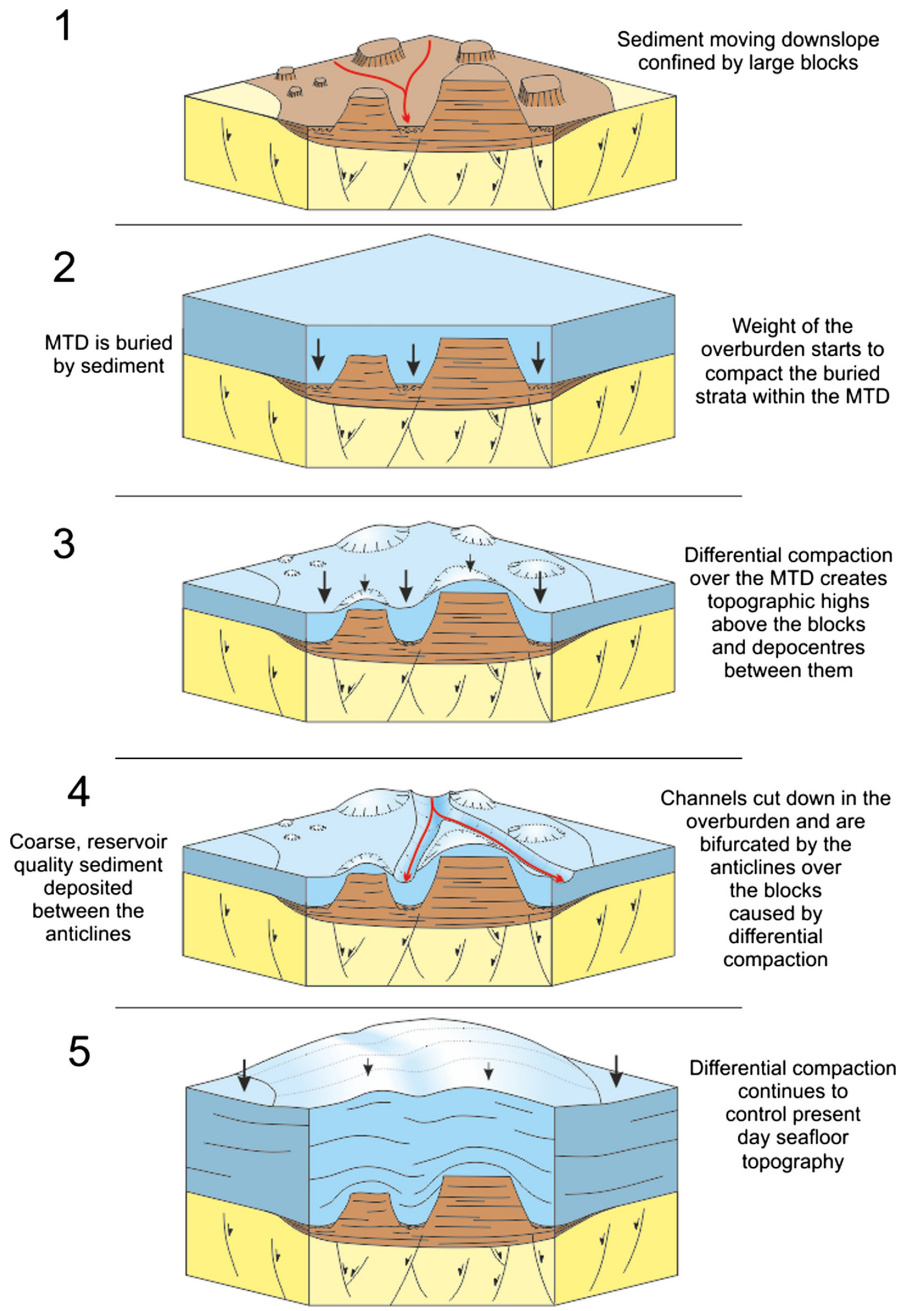

FIGURE 12 Block diagrams showing the evolution of sediment distribution pathways influenced by differential compaction above the studied MTD. Stages 1–5 represent important controls on the distribution in the study area. A tentative scale bar is provided in stage 1

roughness likely controlled subsequent sediment distribution (Alves, 2010; Armitage et al., 2009; Kneller et al., 2016; McAdoo et al., 2004). Chasms between the blocks, ranging from 100 m–1 km wide, confined sediment fairways, as turbidity currents bypassed them downslope (Armitage et al., 2009). Due to their varying heights, the tops of some blocks were still exposed after others had been buried. This is most prominent when comparing the distal blocks to the proximal blocks; there was >100 ms of sediment deposited over the distal blocks before the proximal blocks were buried (Figure 10). Differential compaction over smaller blocks maintained seafloor roughness shortly after burial. It was therefore possible that large, exposed blocks confined sediment fairways in the proximal area, whilst the same sediment fairway was confined by compaction-related anticlines over the smaller blocks in the distal area.

The striations found within the map of H_3 demonstrate the influence the blocks exert on sediment fairways (Figure 5a). As suggested by Gee et al. (2005) and Posamentier (2003), striations can represent sediment pathways. On the map, the sediment fairway is bisected by a slide block; the striations split and divert around the north and south of it (Figure 5a). Directly overlying this fairway is a channel confined by compaction-related anticlines and large blocks in MTD A (Figure 6). The base of these channel lies on horizon H_3 and the upper surface is interpreted as H_4 (Figure 6b). Few blocks were actually exposed on the seafloor at the time H_4 was deposited, but the compaction-related anticlines were still affecting the seafloor topography. We interpret these anticlines to be responsible for confining the channel. Other channels are observed on the interpreted seismic volume (without the striated bases), and they all seem to lie lateral to the blocks (Figure 4b).

The isochron maps agree with the channels seen on seismic sections (Figure 4b and 9). Channels overly the debrites, forming linear features parallel to the flow direction of MTD A. Also, the thickest packages initiate upslope from chasms between the largest blocks (Figure 9). Topographic expression of blocks on the seafloor in the proximal parts of MTD A confined downslope flows, synchronous with compaction-related anticlines over the blocks confining sediments in the distal part. This whole process is summarized on a block diagram in Figure 12.

Trends observed in the width:height graph provide scaling relationships between the stratigraphic elements. The oldest elements (MTD blocks) have the lowest width:height ratio. Younger elements width:height ratios increase (Figure 8). Thus, during progressive burial, the influence slide blocks have on the size of stratigraphic elements diminishes. This is an important conclusion: the interpreted slide blocks can control the dimensions and location of younger, overlying stratigraphic elements, but will only create stratigraphic elements with relatively higher width:height ratios.

8 | CONCLUSIONS

This paper investigated the effects of differential compaction over remnant and rafted blocks within an MTD. In particular, it focused on the evolution and effects of differential compaction on sediment distribution after MTD A was buried. The conclusions are as follows:

1. Differential compaction occurred after the rafted and remnant blocks had been buried by at least 50 ms (~45 m) of sediment, i.e. after the deposition of horizon H_3. We interpret this as the result of lithological contrasts between calcareous blocks from the Caravelas Formation and surrounding debrites.
2. Post burial, differential compaction led to the formation of anticlines and associated depocentres over MTD A. Present-day strata are still deforming over the largest blocks located in the proximal area of MTD A.
3. Differential compaction was not synchronous across the whole of MTD A. Some blocks were still exposed in the proximal areas after others in the distal areas had been buried by >100 ms (~90 m) of sediment.
4. Slide blocks controlled sediment distribution over MTD A: sediment fairways were confined to the areas between the blocks. After differential compaction had occurred, the compaction-related anticlines continued to control sediment distribution downslope. This maintained the seafloor roughness for >5 Ma after MTD A was buried. Figure 6 shows an example of this.
5. Log-log plots of width and height prove that there is a relationship between the size of slide blocks and depocentres. Large blocks can influence the formation of stratigraphic elements in the overburden, which tend to have higher width:height ratios than the blocks. Understanding these relationships can help predict the effects of differential compaction over shallow MTDs in similar passive margins, and where depocentres are likely to form.

We have shown one example of the impact that differential compaction, promoted by a blocky MTD, can have on the seafloor topography and sediment distribution. Seafloor roughness, originally created by the blocks, will be maintained over topographic features if differential compaction occurs after burial. This can potentially confine flows and channels. Smaller depocentres can potentially pond significant volumes of sediment travelling downslope as the channels pass through them.

ACKNOWLEDGEMENTS

The work contained in this paper was conducted during a Ph.D. study undertaken as part of the Natural Environment Research Council (NERC) Centre for Doctoral Training (CDT) in Oil & Gas and is funded by NERC and co-sponsored by Cardiff University, whose support is gratefully acknowledged. We thank CGG© for access and permission to publish examples from their 3D seismic data volumes. We acknowledge Schlumberger (Petrel©) for granting provisions of academic licences to Cardiff's 3D Seismic Lab. We thank the reviewer S. Cardona and another anonymous reviewer for their suggestions and improvements to the initial manuscript, and associate editor R. Bell for their constructive comments and editorial support.

ORCID

Nicholas I. P. Ward http://orcid.org/0000-0002-6688-0296
Tiago M. Alves http://orcid.org/0000-0002-2765-3760
Thomas G. Blenkinsop http://orcid.org/0000-0001-9684-0749

REFERENCES

Alves, T. M. (2010). 3D Seismic examples of differential compaction in mass-transport deposits and their effect on post-failure strata. *Marine Geology*, *271*(3), 212–224. https://doi.org/10.1016/j.margeo.2010.02.014

Alves, T. M., & Cartwright, J. A. (2010). The effect of mass-transport deposits on the younger slope morphology, offshore Brazil. *Marine and Petroleum Geology*, *27*(9), 2027–2036. https://doi.org/10.1016/j.marpetgeo.2010.05.006

Alves, T. M., Cartwright, J., & Davies, R. J. (2009). Faulting of salt-withdrawal basins during early halokinesis: Effects on the Paleogene Rio Doce Canyon system (Espírito Santo Basin, Brazil). *AAPG Bulletin*, *93*(5), 617–652. https://doi.org/10.1306/02030908105

Alves, T. M., Kurtev, K., Moore, G. F., & Strasser, M. (2014). Assessing the internal character, reservoir potential, and seal competence of mass-transport deposits using seismic texture: A geophysical and petrophysical approach. *AAPG Bulletin*, *98*(4), 793–824. https://doi.org/10.1306/09121313117

Armitage, D. A., Romans, B. W., Covault, J. A., & Graham, S. A. (2009). The influence of mass-transport-deposit surface topography on the evolution of turbidite architecture: The Sierra Contreras, Tres Pasos formation (Cretaceous), southern Chile. *Journal of Sedimentary Research*, *79*(5), 287–301.

Asmus, H. E., Gomes, J. B., & Pereira, A. C. B. (1971). Integração geológica regional da bacia do Espírito Santo. *Relatório Interno*, PETROBRAS.

Babonneau, N., Savoye, B., Cremer, M., & Klein, B. (2002). Morphology and architecture of the present canyon and channel system of the Zaire deep-sea fan. *Marine and Petroleum Geology*, *19*(4), 445–467. https://doi.org/10.1016/S0264-8172(02)00009-0

Barker, P. (1983). Tectonic evolution and subsidence history of the Rio-Grande Rise. *Initial Reports of the Deep Sea Drilling Project*, *72*(Dec), 953–976.

Barker, P. F., Buffler, R. T., & Gambôa, L. A. (1983). A seismic-reflection study of the Rio-Grande Rise. *Initial Reports of the Deep Sea Drilling Project*, *72*(Dec), 499–517.

Baudon, C., & Cartwright, J. (2008). The kinematics of reactivation of normal faults using high resolution throw mapping. *Journal of Structural Geology*, *30*, 1072–1084. https://doi.org/10.1016/j.jsg.2008.04.008

Beaubouef, R., & Abreu, V. (2010). MTCs of the Brazos-Trinity slope system; thoughts on the sequence stratigraphy of MTCs and their possible roles in shaping hydrocarbon traps. In D. C. Mosher, R. C. Shipp, L. Mos-cardelli, J. D. Chaytor, C. D. P. Baxter, H. J. Lee, & R. Urgeles (Eds.), *Submarine mass movements and their consequences* (pp. 475–490). Dordrecht, The Netherlands: Springer.

Bjørlykke, K., & Høeg, K. (1997). Effects of burial diagenesis on stresses, compaction and fluid flow in sedimentary basins. *Marine and Petroleum Geology*, *14*(3), 267–276. https://doi.org/10.1016/S0264-8172(96)00051-7

Chang, H. K., Kowsmann, R. O., Figueiredo, A. M. F., & Bender, A. (1992). Tectonics and stratigraphy of the East Brazil Rift system: An overview. *Tectonophysics*, *213*(1), 97–138. https://doi.org/10.1016/0040-1951(92)90253-3

Clark, J. D., & Pickering, K. T. (1996). Architectural elements and growth patterns of submarine channels: Application to hydrocarbon exploration. *AAPG Bulletin*, *80*(2), 194–220.

Corfield, S., & Sharp, I. (2000). Structural style and stratigraphic architecture of fault propagation folding in extensional settings: A seismic example from the Smørbukk area, Halten Terrace, Mid-Norway. *Basin Research*, *12*(3–4), 329–341. https://doi.org/10.1046/j.1365-2117.2000.00133.x

Cosgrove, J., & Ameen, M. (1999). A comparison of the geometry, spatial organization and fracture patterns associated with forced folds and buckle folds. *Geological Society, London, Special Publications*, *169*(1), 7–21. https://doi.org/10.1144/GSL.SP.2000.169.01.02

Davison, I. (1999). Tectonics and hydrocarbon distribution along the Brazilian South Atlantic margin. *Geological Society, London, Special Publications*, *153*(1), 133–151. https://doi.org/10.1144/GSL.SP.1999.153.01.09

Davison, I. (2007). Geology and tectonics of the South Atlantic Brazilian salt basins. *Geological Society, London, Special Publications*, *272*(1), 345–359. https://doi.org/10.1144/GSL.SP.2007.272.01.18

Demercian, S. Szatmari, P., &Cobbold, P. R. (1993). Style and pattern of salt diapirs due to thin-skinned gravitational gliding, Campos and Santos basins, offshore Brazil. *Tectonophysics*, *228*(3), 393–433. https://doi.org/10.1016/0040-1951(93)90351-J

Deptuck, M. E., Sylvester, Z., Pirmez, C., & O'Byrne, C. (2007). Migration–aggradation history and 3-D seismic geomorphology of submarine channels in the Pleistocene Benin-major Canyon, western Niger Delta slope. *Marine and Petroleum Geology*, *24*(6), 406–433. https://doi.org/10.1016/j.marpetgeo.2007.01.005

Di Celma, C. N., Brunt, R. L., Hodgson, D. M., Flint, S. S., & Kavanagh, J. P. (2011). Spatial and temporal evolution of a Permian submarine slope channel–levee system, Karoo Basin, South Africa. *Journal of Sedimentary Research*, *81*(8), 579–599. https://doi.org/10.2110/jsr.2011.49

Dowdeswell, J. A., Ottesen, D., Rise, L., & Craig, J. (2007). Identification and preservation of landforms diagnostic of past ice-sheet activity on continental shelves from three-dimensional seismic evidence. *Geology*, *35*(4), 359–362. https://doi.org/10.1130/G23200A.1

Dugan, B., & Flemings, P. B. (2000). Overpressure and fluid flow in the New Jersey continental slope: Implications for slope failure and cold seeps. *Science*, *289*(5477), 288–291. https://doi.org/10.1126/science.289.5477.288

Dykstra, M., Garyfalou, K., Kertznus, V., Kneller, B., Milana, J. P., Molinaro, M., … Thompson, P. (2011). Mass-transport deposits: Combining outcrop studies and seismic forward modeling to understand lithofacies distributions, deformation, and their seismic expression. *SEPM Special Publication*, *96*, 293–310.

Fiduk, J. C., Brush, E. R., Anderson, L. E., Gibbs, P. B., & Rowan, M. G. (eds.) (2004). Salt deformation, magmatism, and hydrocarbon prospectivity in the Espirito Santo Basin, offshore Brazil. Salt-sediment interactions and hydrocarbon prospectivity: Concepts, applications, and case studies for the 21st century: Proceedings of Gulf Coast Section SEPM Foundation Bob F. Perkins Research Conference. SEPM.

Gamboa, D., & Alves, T. M. (2015a). Spatial and dimensional relationships of submarine slope architectural elements: A seismic-scale analysis from the Espírito Santo Basin (SE Brazil). *Marine and Petroleum Geology*, *64*, 43–57. https://doi.org/10.1016/j.marpetgeo.2015.02.035

Gamboa, D., & Alves, T. M. (2015b). Three-dimensional fault meshes and multi-layer shear in mass-transport blocks: Implications for fluid flow on continental margins. *Tectonophysics*, *647*, 21–32. https://doi.org/10.1016/j.tecto.2015.02.007

Gamboa, D., & Alves, T. M. (2016). Bi-modal deformation styles in confined mass-transport deposits: Examples from a salt minibasin in SE Brazil. *Marine Geology*, *379*, 176–193. https://doi.org/10.1016/j.margeo.2016.06.003

Gamboa, D., Alves, T., Cartwright, J., & Terrinha, P. (2010). MTD distribution on a 'passive'continental margin: The Espírito Santo Basin (SE Brazil) during the Palaeogene. *Marine and Petroleum Geology*, *27*(7), 1311–1324. https://doi.org/10.1016/j.marpetgeo.2010.05.008

Gee, M., Gawthorpe, R. L., Bakke, K., & Friedmann, S. J. (2007). Seismic geomorphology and evolution of submarine channels from the Angolan continental margin. *Journal of Sedimentary Research*, *77*(5), 433–446. https://doi.org/10.2110/jsr.2007.042

Gee, M., Gawthorpe, R. L., & Friedmann, J. S. (2005). Giant striations at the base of a submarine landslide. *Marine Geology*, *214*(1), 287–294. https://doi.org/10.1016/j.margeo.2004.09.003

Gee, M., Gawthorpe, R. L., & Friedmann, S. J. (2006). Triggering and evolution of a giant submarine landslide, offshore Angola, revealed by 3D seismic stratigraphy and geomorphology. *Journal of Sedimentary Research*, *76*(1), 9–19. https://doi.org/10.2110/jsr.2006.02

Gong, C., Wang, Y., Steel, R. J., Peakall, J., Zhao, X., & Sun, Q. (2016). Flow processes and sedimentation in unidirectionally migrating deep-water channels: From a three-dimensional seismic perspective. *Sedimentology*, *63*(3), 645–661. https://doi.org/10.1111/sed.12233

Hampton, M. A., Lee, H. J., &Locat, J. (1996). Submarine landslides. *Reviews of geophysics*, *34*(1), 33–59. https://doi.org/10.1029/95RG03287

Hardy, S., & McClay, K. (1999). Kinematic modelling of extensional fault-propagation folding. *Journal of Structural Geology*, *21*(7), 695–702. https://doi.org/10.1016/S0191-8141(99)00072-3

Hunt, D., & Swarbrick, R. E. (1996). Compaction as a primary control on the architecture and development of depositional sequences: Conceptual framework, applications and implications. *Geological Society, London, Special Publications*, *104*(1), 321–345. https://doi.org/10.1144/GSL.SP.1996.104.01.18

Kneller, B., Dykstra, M., Fairweather, L., & Milana, J. P. (2016). Mass-transport and slope accommodation: Implications for turbidite sandstone reservoirs. *AAPG Bulletin*, *100*(2), 213–235. https://doi.org/10.1306/09011514210

Kumar, N., Gamboa, L. A. P., Schreiber, B. C., & Mascle, J. (1977). Geologic history and origin of Sao Paulo Plateau (Southeastern Brazilian Margin), comparison with the Angolan margin and the early evolution of the Northern South Atlantic. *Initial Reports of the Deep Sea Drilling Program*, *39*, 927–945.

Lee, S. E., Talling, P. J., Ernst, G. G., & Hogg, A. J. (2002). Occurrence and origin of submarine plunge pools at the base of the US continental slope. *Marine Geology*, *185*(3), 363–377. https://doi.org/10.1016/S0025-3227(01)00298-5

Maillard, A., Gaullier, V., Vendeville, B. C., & Odonne, F. (2003). Influence of differential compaction above basement steps on salt tectonics in the Ligurian-Provençal Basin, northwest Mediterranean. *Marine and Petroleum Geology*, *20*(1), 13–27. https://doi.org/10.1016/S0264-8172(03)00022-9

Masson, D. G., Harbitz, C. B., Wynn, R. B., Pedersen, G., & Løvholt, F. (2006). Submarine landslides: Processes, triggers and hazard prediction. *Philosophical Transactions of the Royal Society of London A: Mathematical, Physical and Engineering Sciences*, *364*(1845), 2009–2039. https://doi.org/10.1098/rsta.2006.1810

McAdoo, B. G., Capone, M. K., & Minder, J. (2004). Seafloor geomorphology of convergent margins: implications for Cascadia seismic hazard. *Tectonics*, *23*(6), TC6008.

McHargue, T., Pyrcz, M. J., Sullivan, M. D., Clark, J. D., Fildani, A., Romans, B. W., … Drinkwater, N. J. (2011). Architecture of turbidite channel systems on the continental slope: Patterns and predictions. *Marine and Petroleum Geology*, *28*(3), 728–743. https://doi.org/10.1016/j.marpetgeo.2010.07.008

Meisling, K. E., Cobbold, P. R., & Mount, V. S. (2001). Segmentation of an obliquely rifted margin, Campos and Santos basins, southeastern Brazil. *AAPG Bulletin*, *85*(11), 1903–1924.

Minisini, D., Trincardi, F., Asioli, A., Canu, M., & Foglini, F. (2007). Morphologic variability of exposed mass-transport deposits on the eastern slope of Gela Basin (Sicily channel). *Basin Research*, *19*(2), 217–240. https://doi.org/10.1111/j.1365-2117.2007.00324.x

Mohriak, W., Nemčok, M., & Enciso, G. (2008). South Atlantic divergent margin evolution: Rift-border uplift and salt tectonics in the basins of SE Brazil. *Geological Society, London, Special Publications*, *294*(1), 365–398. https://doi.org/10.1144/SP294.19

Moscardelli, L., & Wood, L. (2008). New classification system for mass transport complexes in offshore Trinidad. *Basin research*, *20*(1), 73–98. https://doi.org/10.1111/j.1365-2117.2007.00340.x

Newton, C. S., Shipp, R. C., Mosher, D. C., & Wach, G. D. (2004). Importance of mass transport complexes in the Quaternary development of the Nile Fan, Egypt. Offshore Technology Conference. Offshore Technology Conference.

Ojeda, H. (1982). Structural framework, stratigraphy, and evolution of Brazilian marginal basins. *AAPG Bulletin*, *66*(6), 732–749.

Omosanya, K. O., & Alves, T. M. (2013). A 3-dimensional seismic method to assess the provenance of Mass-Transport Deposits (MTDs) on salt-rich continental slopes (Espírito Santo Basin, SE Brazil). *Marine and Petroleum Geology*, *44*, 223–239. https://doi.org/10.1016/j.marpetgeo.2013.02.006

Omosanya, K. D. O., & Alves, T. M. (2014). Mass-transport deposits controlling fault propagation, reactivation and structural decoupling on continental margins (Espírito Santo Basin, SE Brazil). *Tectonophysics*, *628*, 158–171. https://doi.org/10.1016/j.tecto.2014.04.045

Pickering, K. T., & Corregidor, J. (2005). Mass transport complexes and tectonic control on confined basin-floor submarine fans, Middle Eocene, south Spanish Pyrenees. *Geological Society, London, Special Publications*, *244*(1), 51–74. https://doi.org/10.1144/GSL.SP.2005.244.01.04

Pickering, K., & Hiscott, R. (2015). *Deep marine systems: Processes, deposits, environments, tectonic and sedimentation*. New Jersey: Wiley-Blackwell.

Posamentier, H. W. (2003). Depositional elements associated with a basin floor channel-levee system: Case study from the Gulf of Mexico. *Marine and Petroleum Geology*, *20*(6), 677–690. https://doi.org/10.1016/j.marpetgeo.2003.01.002

Posamentier, H. W., & Kolla, V. (2003). Seismic geomorphology and stratigraphy of depositional elements in deep-water settings. *Journal of Sedimentary Research*, *73*(3), 367–388. https://doi.org/10.1306/111302730367

Prather, B. E. (2003). Controls on reservoir distribution, architecture and stratigraphic trapping in slope settings. *Marine and Petroleum Geology*, *20*(6), 529–545. https://doi.org/10.1016/j.marpetgeo.2003.03.009

Qin, Y., Alves, T. M., Constantine, J., & Gamboa, D. (2017). The role of mass wasting in the progressive development of submarine channels (Espirito Santo Basin, SE Brazil). *Journal of Sedimentary Research*, *87*, 500–516. https://doi.org/10.2110/jsr.2017.18

Rise, L., Olesen, O., Rokoengen, K., Ottesen, D., & Riis, F. (2004). Mid-Pleistocene ice drainage pattern in the Norwegian Channel imaged by 3D seismic. *Quaternary Science Reviews*, *23*(23), 2323–2335. https://doi.org/10.1016/j.quascirev.2004.04.005

Rusciadelli, G., & Di Simone, S. (2007). Differential compaction as a control on depositional architectures across the Maiella carbonate platform margin (central Apennines, Italy). *Sedimentary Geology*, *196*(1), 133–155. https://doi.org/10.1016/j.sedgeo.2006.06.006

Sharp, I. R., Gawthorpe, R. L., Underhill, J. R., & Gupta, S. (2000). Fault-propagation folding in extensional settings: Examples of structural style and synrift sedimentary response from the Suez rift, Sinai, Egypt. *GSA Bulletin*, *112*(12), 1877–1899. https://doi.org/10.1130/0016-7606(2000)112<1877:FPFIES>2.0.CO;2

Shultz, M. R., Fildani, A., Cope, T. D., & Graham, S. A. (2005). Deposition and stratigraphic architecture of an outcropping ancient slope system: Tres Pasos Formation, Magallanes Basin, southern Chile. *Geological Society, London, Special Publications*, *244*(1), 27–50. https://doi.org/10.1144/GSL.SP.2005.244.01.03

Stigall, J., & Dugan, B. (2010). Overpressure and earthquake initiated slope failure in the Ursa region, northern Gulf of Mexico. *Journal of Geophysical Research: Solid Earth*, *115*(B4).

Trask, P. D. (1931). Compaction of sediments. *AAPG Bulletin*, *15*(3), 271–276.

Viana, A., Figueiredo, A., Faugres, J. C., Lima, A., Gonthier, E., Brehme, I., & Zaragosi, S. (2003). The Sao Tom deep-sea turbidite system (southern Brazil Basin): Cenozoic seismic stratigraphy and sedimentary processes. *AAPG Bulletin*, *87*(5), 873–894. https://doi.org/10.1306/12100201048

Weller, J. M. (1959). Compaction of sediments. *AAPG Bulletin*, *43*(2), 273–310.

SUPPORTING INFORMATION

Additional Supporting Information may be found online in the supporting information tab for this article.

How to cite this article: Ward NIP, Alves TM, Blenkinsop TG. Submarine sediment routing over a blocky mass-transport deposit in the Espírito Santo Basin, SE Brazil. *Basin Res*. 2018;00:1–19. https://doi.org/10.1111/bre.12282